Geophysical Research Letters

RESEARCH LETTER
10.1029/2021GL093564

Key Points:

- Onset of induced earthquakes in the Fort Worth Basin occurred with pore pressure increases of ~0.01–0.36 MPa from wastewater injection
- Pore pressure increase in the slip potential of the seismogenic faults indicates that the instability threshold is 17%–24% for this system
- Slip potential of faults that became seismogenic is similar to those that have not ruptured, indicating inherent differences in sensitivity

Supporting Information:

Supporting Information may be found in the online version of this article.

Correspondence to:

P. H. Hennings,
peter.hennings@beg.utexas.edu

Citation:

Hennings, P. H., Nicot, J.-P., Gao, R. S., DeShon, H. R., Lund Snee, J.-E., Morris, A. P., et al. (2021). Pore pressure threshold and fault slip potential for induced earthquakes in the Dallas-Fort Worth area of north central Texas. *Geophysical Research Letters*, *48*, e2021GL093564. https://doi.org/10.1029/2021GL093564

Received 27 MAR 2021
Accepted 11 MAY 2021

Pore Pressure Threshold and Fault Slip Potential for Induced Earthquakes in the Dallas-Fort Worth Area of North Central Texas

P. H. Hennings[1], J.-P. Nicot[1], R. S. Gao[1], H. R. DeShon[2], J.-E. Lund Snee[3], A. P. Morris[4], M. R. Brudzinski[5], E. A. Horne[1], and C. Breton[1]

[1]Jackson School of Geosciences, Bureau of Economic Geology, The University of Texas at Austin, Austin, TX, USA, [2]Department of Earth Sciences, Southern Methodist University, Dallas, TX, USA, [3]Geosciences and Environmental Change Science Center, U.S. Geological Survey, Denver, CO, USA, [4]Alan Morris Consulting, Traverse City, MI, USA, [5]Department of Geology and Environmental Earth Science, Miami University, Oxford, OH, USA

Abstract Earthquakes were induced in the Fort Worth Basin from 2008 through 2020 by increase in pore pressure from injection of oilfield wastewater (SWD). In this region and elsewhere, a missing link in understanding the mechanics of causation has been a lack of comprehensive models of pore pressure evolution (ΔPp) from SWD. We integrate detailed earthquake catalogs, ΔPp, and probabilistic fault slip potential (FSP) and find that faults near large-scale SWD operations became unstable early, when ΔPp reached ~0.31 MPa and FSP reached 0.24. Faults farther from SWD became unstable later, when FSP reached 0.17 and at much smaller ΔPp. Earthquake sequences reactivated with mean ΔPp of ~0.05 MPa. The response of faults shows strong variability, with many remaining stable at higher ΔPp and few that became seismogenic at smaller changes. As ΔPp spread regionally, an ever-increasing number of faults were impacted and the most sensitive became unstable.

Plain Language Summary Increases in subsurface fluid pressure following years of deep disposal of oilfield wastewater are widely accepted to have caused earthquakes from 2008 through 2020 in the Fort Worth Basin (FWB) of north-central Texas, underlying the population centers of the Dallas-Fort Worth metropolitan area, were caused by increases in subsurface fluid pressure following years of deep disposal of oilfield wastewater. No earthquakes were reported in the area prior to 2008. Increasing the fluid pressure in subsurface reservoirs containing faults can cause the faults to become unstable and slip, producing earthquakes. A missing link to understanding the cause of these earthquakes is not knowing how much the fluid pressures have increased, and which geographic areas have been affected. This research combines several lines of evidence to show how the fluid pressure from deep injection increased over time and space leading to the increase in earthquakes. The changes in fluid pressure that made the faults unstable is surprisingly low, the subsurface region affected by the pressure change is large, and the natural sensitivity of the faults has significant variability. This work provides a critical component to understanding the specific conditions leading to induced seismicity in the FWB, which can be applied to similar cases elsewhere.

1. Introduction

It is well established that the increase in seismicity in the Fort Worth Basin (FWB) from 2008 through its peak in 2015, and continuing recently at far lower magnitudes and rates, was caused by deep disposal of oilfield wastewater (SWD) associated with development and production of the Barnett Shale (Figures 1 and 2) (Frohlich et al., 2016; Gao et al., 2021; Hennings et al., 2019; Hornbach et al., 2015, 2016; Magnani et al., 2017; Quinones et al., 2019; Scales et al., 2017). Discussion continues regarding the specific mechanisms that acted to induce multiple episodes of fault slip and earthquakes in the FWB, herein called earthquake sequences (ESs). Hennings et al. (2019), Hornbach et al. (2015, 2016), Lund Snee and Zoback (2016), and Ogwari et al. (2018) emphasized the role of pressure diffusion and reduction in effective normal stress acting on faults. Chen et al. (2018), Haddad and Eichhubl (2020), and Zhai and Shirzaei (2018) added that poroelastic stress change from pore pressure increase (ΔPp) contributes. No works to date have implicated hydraulic fracturing as a direct agent of causation in the FWB.

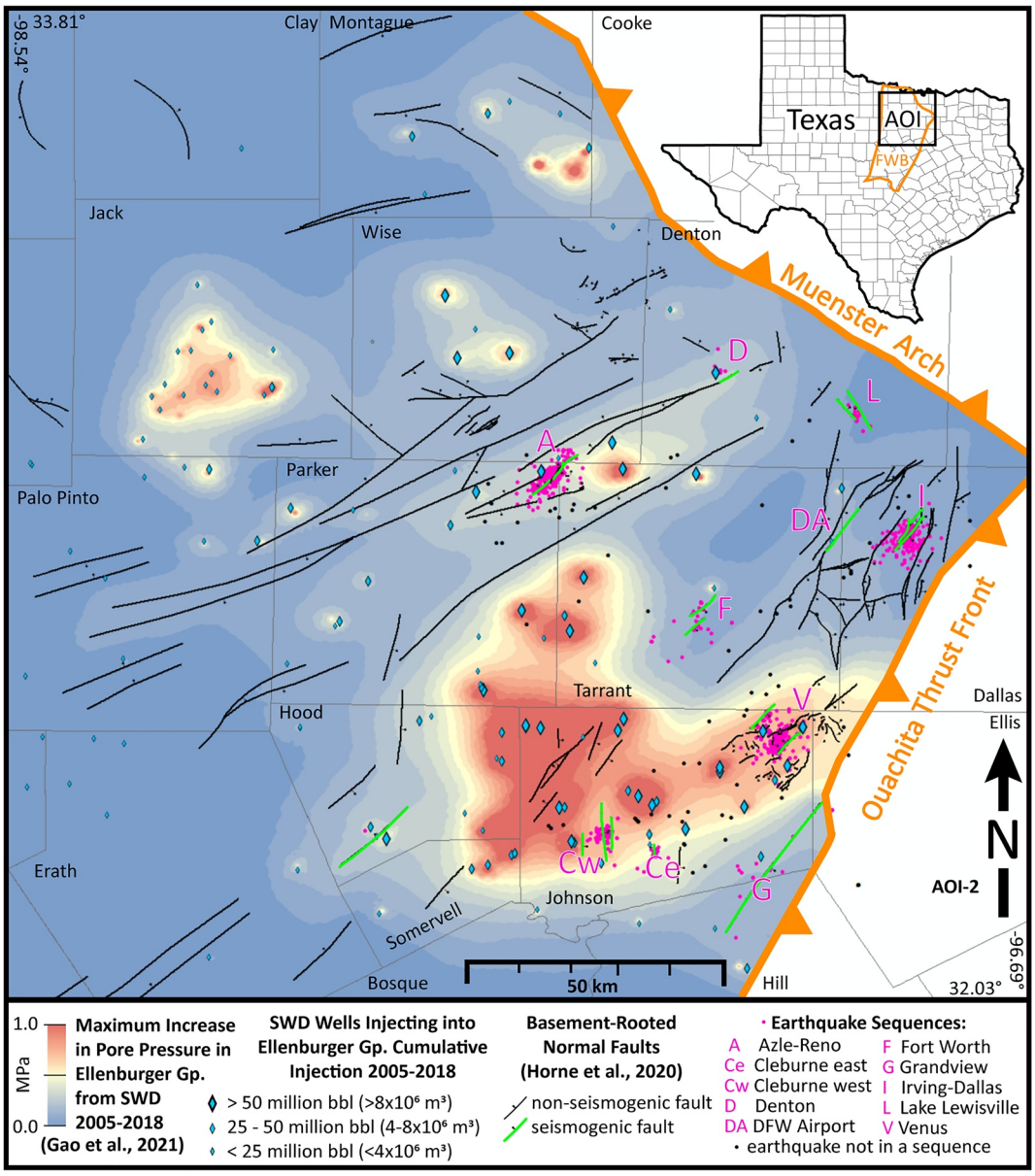

Figure 1. Map of the area of interest in the Fort Worth Basin showing saltwater disposal wells and cumulative injected volumes, the entire record of seismicity from SMU NTXES, the earthquake sequences that we study here, traces of basement-rooted faults from Horne et al. (2020), and the distribution of the maximum ΔPp at the basement-sediment interface from the Gao et al. (2021) hydrogeologic model.

Clearly, having a comprehensive assessment of the relationship between ΔPp associated with SWD and earthquakes would provide a substantial benefit for investigating the specific rupture mechanisms in the FWB and elsewhere. Applications include regulating SWD and adjusting petroleum operations to mitigate earthquakes.

Direct measurements of subsurface pore pressure in close spatiotemporal relation with fault rupture are generally not publicly available and the few that exist (e.g., Scales et al., 2017) do not provide a useful sample of the FWB as a geologic system. Using a local model of the Azle (A) ES, Hornbach et al. (2015) found that pore pressures may have increased by up to 0.2 MPa prior to earthquake onset. Using diffusion models at regional scale, Gono et al. (2015) found that ΔPp may have ranged 2.07–4.14 MPa in close proximity to the first ESs to develop (DA and Ce, Figure 1).

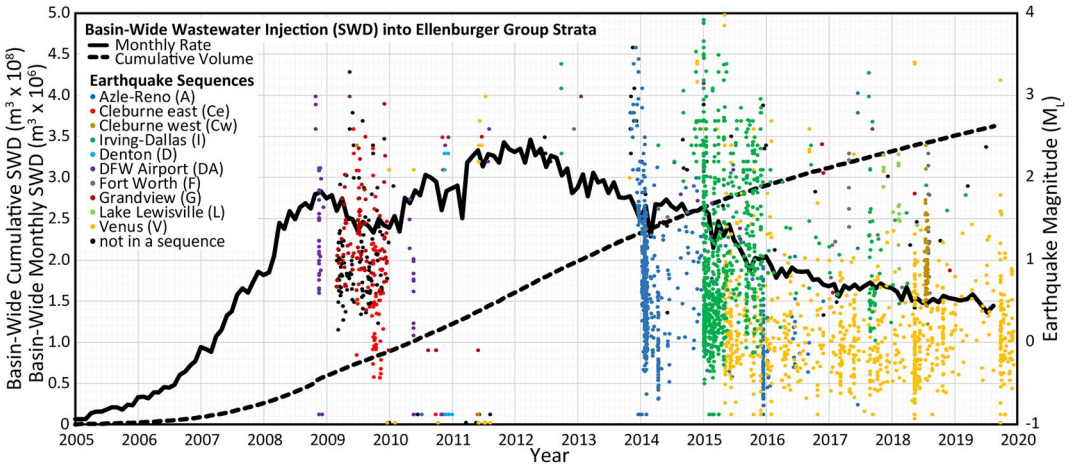

Figure 2. History of saltwater disposal (SWD) and magnitude of earthquakes within the Fort Worth Basin as divided into the sequences studied here. Earthquakes of unknown magnitude are posted at M_L −0.9. SWD data from the Railroad Commission of Texas [last accessed Dec 31, 2020] provide complete records for all wells through September 2019.

A common attribute of prior works that address earthquake causation using pore pressure analyses in the FWB is the use of highly simplified geologic and hydrologic models. However, the subsurface intervals used for disposal, the Paleozoic Ellenburger Group, is known to be geologically complex in its layering, distribution of facies, matrix properties, distribution of karst, fractures, and faults, all of which must be considered in any concerted effort to understand the spatiotemporal association between ΔPp from SWD, and the geomechanical impact leading to earthquake inducement.

Our purpose here is to integrate the most complete earthquake data available, comprehensive geologic inputs, and thoroughly developed models to assess the role that ΔPp played in altering the natural earthquake hazard and inducing earthquakes at the local to regional scale in the FWB, with application locally and for understanding analogous systems. We do not posit that alteration of effective stress from ΔPp is *the* singular physical cause of fault rupture. Rather, ΔPp is the causative agent, and given the available modeling and data collection practices, subsurface practitioners commonly focus on ΔPp to assess the hazard of induced seismicity. Elevated pore pressure can be viewed as an indicator of rupture likelihood if all other required factors are satisfied.

2. Data and Methods

To investigate the onset and continued activity of the key earthquake sequences in the FWB and the spatial and temporal association with ΔPp from SWD, we assess the relationships between four datasets: (a) an earthquake catalog expanded in key areas by template matching, (b) spatiotemporal comparison of modeled ΔPp with ES development and the response of faults that did and did not host earthquakes, (c) comparison of the deterministic sensitivity of slip for 3D surfaces of the faults that hosted earthquakes, and (d) comparison of the evolution of the probabilistic fault slip potential (FSP) of the faults that hosted earthquakes.

2.1. Earthquake History in the FWB

The history of monitoring and cataloging induced earthquakes in the FWB is summarized by DeShon et al. (2018) and Quinones et al. (2019). For this analysis, we use regional earthquake data from U.S. Geological Survey ComCat [last accessed Mar 22, 2021], Frohlich (2012), SMU NTXES [last accessed Mar 22, 2021] (DeShon et al., 2018; Quinones et al., 2019), and local studies (Justinic et al., 2013) including those with template matching (Ogwari et al., 2018; Scales et al., 2017). Earthquake catalogs in the A and Irving (I) ES areas were also extended by template matching as described in Text S1. The combined earthquake catalog we use is shown in summary form in Figures 1 and 2 and is available in tabular form as Dataset 1. Figure 3 shows the distribution of earthquake magnitudes as a function of time within each ES.

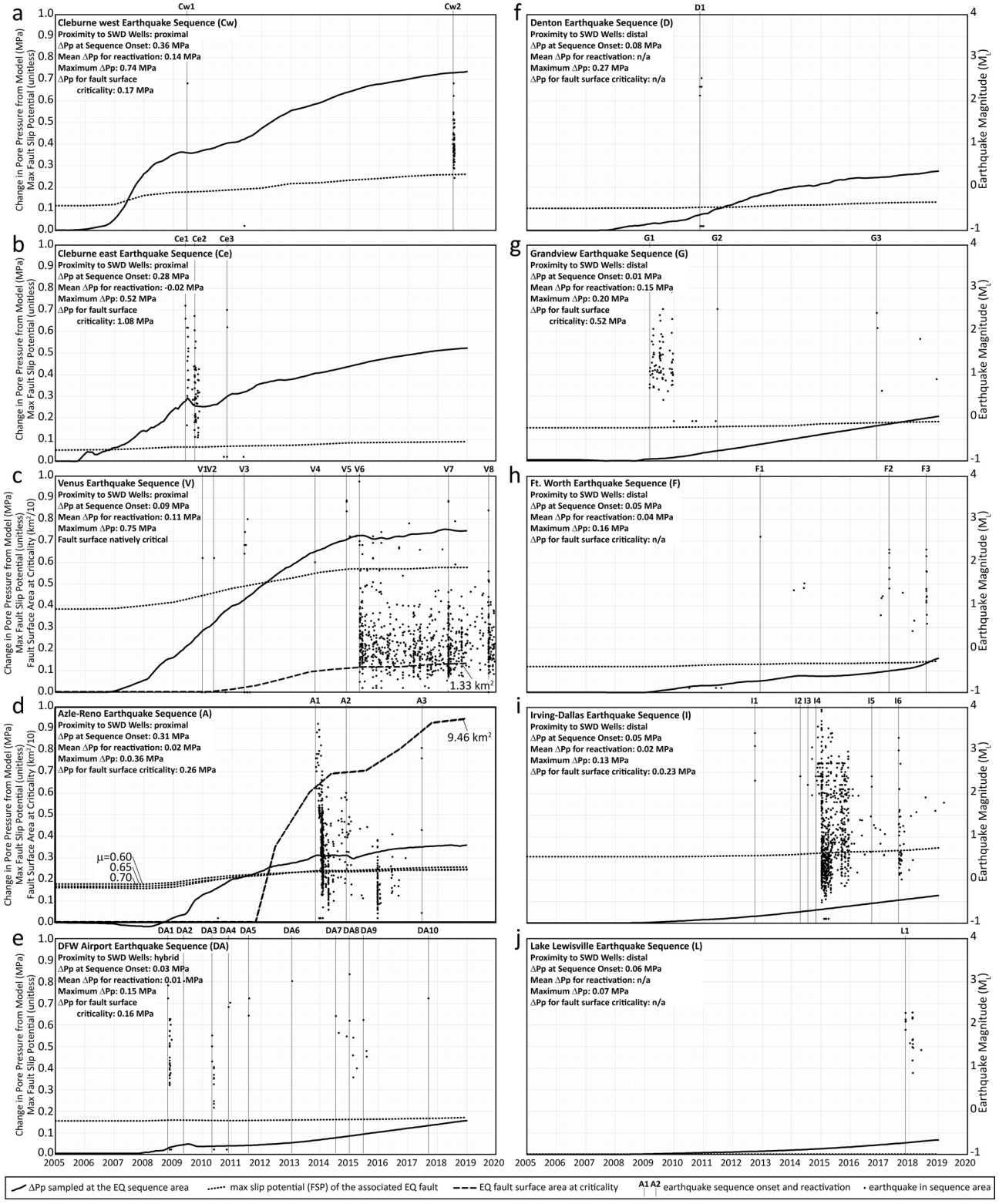

Figure 3. Temporal evolution of factors at the studied earthquake sequence (ES) areas showing earthquake history, interpreted ES onset and reactivation, local ΔPp from the hydrogeologic model, deterministic estimate of the surface area of the seismogenic faults that were critically stressed (c and d only), and slip potential (FSP) of the seismogenic faults. For the FSP analysis, the coefficient of friction (μ) and its uncertainty range is 0.7 ± 0.05 (as outlined in Table S2) for all areas, but the (inconsequential) effect of changing μ is illustrated for the A ES (d).

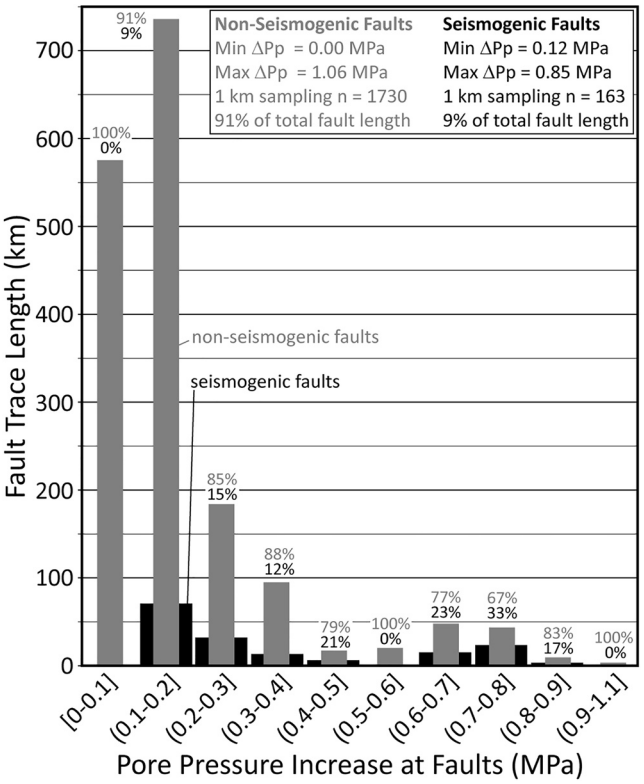

Figure 4. Distribution of maximum ΔPp experienced by the seismogenic and non-seismogenic faults between the years 2005–2019 in the area of interest. The percentages show the splits within each ΔPp bin between seismogenic and non-seismogenic faults.

Earthquakes in the FWB occur primarily in discrete spatial sequences (Quinones et al., 2019) on faults recently interpreted by Hennings et al. (2019) and Horne et al. (2020) (Figures 1 and 2). Most earthquakes have produced normal faulting mechanisms with NE-striking nodal planes (Magnani et al., 2017; Quinones et al., 2018). The vast majority of the earthquakes occurred beneath the sedimentary succession in poorly understood Proterozoic crystalline and metamorphic rocks.

We study 10 of the ESs here. The behavior of the ES can be broadly classified as temporally discrete, with earthquakes most commonly occurring over a time span of a few days to weeks (D, L, Ce); discrete and episodic (Cw, A, DA, F); and diffuse and more complex (G, V, I) (Table S1). However, variations in the timing and effectiveness of seismic station placement have an impact on the robustness of this classification scheme. We investigate the discrete activity or reactivation of each ES. We define a reactivation as a cessation in activity of at least 3 months followed by significant renewed activity with 1+ earthquakes of M_L2.0+. As described in Section 3.2, we also characterize the ESs by their proximity to areas of significant SWD.

2.2. Pore Pressure History at the Earthquake Sequences and the Faults

We use the history of ΔPp in the FWB due to SWD as derived from the hydrogeologic modeling by Gao et al. (2021) (ΔPp model), to compare to the earthquake history and the evolution of fault criticality and FSP. The ΔPp model employs comprehensive and integrated deterministic geologic inputs and thorough geostatistical modeling for populating reservoir fluid flow properties in 3D. The matrix and facies information are from Smye et al. (2019). Fault data are from Hennings et al. (2019) and Horne et al. (2020) who also point out that the faults are remarkably uniform in their structural characteristics such as strike, dip, and orientation with respect to the in situ stress state. The ΔPp model was calibrated using established reservoir engineering approaches and was thoroughly tested for its sensitivity to key input data. The model incorporates a high level of geologic heterogeneity including multiple scales of fracture and fault permeability. Gao et al. (2021) found that major faults in the ΔPp model, including those that became seismogenic, serve to preferentially and significantly diffuse pore pressure away from areas of SWD. The earthquakes occurred mainly in the basement rock along faults that cut directly from SWD injection intervals in the Ellenburger Group downward into basement. However, the faulted and fractured basement is not amenable to high-resolution ΔPp modeling given current abilities for parameterization. Therefore, for this analysis, we sampled the average monthly pressure for the ES areas in the layer above basement (Figure 3). We have confidence in the ΔPp model results for this layer, which is directly connected to basement by faults. Gao et al. (2021) show that the Ellenburger Group is thoroughly karstified, fractured and faulted creating strong heterogeneity and anisotropy in permeability and it is therefore not amenable to straightforward poroelastic parameterization beyond the near-wellbore scale. In their study of the FWB, Zhai and Shirzaei (2018) show that changes in effective stress regionally are an order of magnitude larger than from poroelastic stress. Therefore, we focus our analysis on effective stress and urge future research to use this work as a basis to further investigate the impact of poroelastic stressing from ΔPp.

To investigate the distribution of ΔPp as experienced by the faults in the area of interest (AOI), we sampled the distribution of maximum ΔPp using the traces of the faults at the basement/sediment contact (unconformity) from Horne et al. (2020). As illustrated in Figure S1, we resampled the grid of maximum ΔPp from Gao et al. (2021) at a 152 m spacing, and then extracted the pressure along the fault traces with nodes spaced at 1 km. The distribution of ΔPp experienced by the seismogenic and non-seismogenic faults is shown in Figure 4. We note however that as per Hennings et al. (2019) and Horne et al. (2020), this fault dataset is biased to capture all of the seismogenic faults that were interpreted from the ES areas but, due to scarcity

of publicly available data with which to interpret faults uniformly throughout the basin, it underrepresents non-seismogenic faults.

2.3. Evolution of the Critical State of Fault Surfaces

To assess whether our approach of sampling ΔPp from the sediment layer above basement yields satisfactory results we investigate the change in the surface area of the seismogenic faults that became critically stressed due to the evolving ΔPp. We also include this deterministic analysis to provide context for the analysis of FSP as described below. The question we are asking is: if we use a simple and commonly employed approach, based on our knowledge of the fault surfaces that hosted the ESs and the stress state, to what degree do the faults become critically stressed with ΔPp? The fault surface criticality analysis method is described in Table S2.

2.4. Evolution of Fault Slip Potential

Hennings et al. (2019) estimated the native (pre-injection) FSP for the entire population of faults in the FWB, as well as the FSP for a hypothetical uniform ΔPp of +1 MPa due to SWD. Here we employ ΔPp estimates over time to investigate the sensitivity of the faults that did and did not host earthquakes in the FWB and the degree to which that sensitivity changed, probabilistically, prior to and during the studied ESs in the FWB. The analysis was conducted using the FSP v.1.07 software tool (Walsh et al., 2017), following the approaches of Hennings et al. (2019), Lund Snee and Zoback (2018), and Walsh and Zoback (2016). The FSP analysis method is more fully described in Table S2. In Figure 3, we summarize the yearly evolution of the maximum FSP reached at each ES area. We choose to highlight the maximum FSP because the more sensitive fault segments would be the most likely to be reactivated first due to ΔPp.

3. Results and Discussion

3.1. Expanded Earthquake Catalog

In the FWB, local seismic networks were deployed in 2008–2009 and 2013–2019 in response to felt earthquakes and provided improved documentation of some ESs (DeShon et al., 2018). ES-specific studies of V (Scales et al., 2017) and DA (Ogwari et al., 2018) include matched filter and template-based catalog expansions, respectively, to identify events prior to local network deployments. In this study, earthquakes in the A and I sequence areas were extended by template matching following the method of Skoumal et al. (2014, 2015), which resulted in increases in the number of cataloged events by 52% and 47%, respectively. Of particular importance to this study, template matching using pre-existing regional seismometers enabled better estimation of the onset of seismicity for comparison with ΔPp. The new template catalogs are archived in online Dataset 1.

3.2. Pore Pressure Increase at Faults, Earthquake Onset, and Reactivation

In the AOI, 163 km of fault trace became seismogenic as compared to 1,730 km of trace that remained non-seismogenic over the period of ΔPp from SWD. The distribution of these two populations within each range of ΔPp is complex and there is no straightforward behavior of faults becoming preferentially seismogenic at higher ΔPp (Figure 4). Two examples illustrate this point: for the regions of the AOI that experienced a total ΔPp of 0.2–0.3 MPa, 15% of the faults became seismogenic and in the regions that experienced a total ΔPp of 0.7–0.8 MPa, 33% of the faults became seismogenic. Several faults became seismogenic in areas that experienced very small ΔPp, mainly in Tarrant, Dallas, and Denton Counties (Figure 1). Moreover, many faults did not become seismogenic in areas that experienced large ΔPp, most notably in the portions of Johnson County where maximum ΔPp was greater than or equal to 1 MPa. A more important aspect of these data is that many more kilometers of fault trace length did not become seismogenic as compared to the trace length that did, at all levels of ΔPp.

Comparing the ΔPp history to the time of ES onset and reactivation, we observe two classes of behavior spatially (Figure 3, Table S1). The V, Cw, Ce, and A sequences in the west and south of the AOI are *proximal*,

meaning that they are within few kilometers of multiple SWD wells with cumulative injection that exceeded 4×10^6 m^3 (25 million bbl) prior to, or during ES activity (Figure 1). The ΔPp history of the *proximal* areas is complex with short-term variations in ΔPp reflecting changing SWD operations nearby (Figures 3a–3d), especially as earthquakes near SWD sites prompted operators to alter disposal practices. As of January 2019, the rate of ΔPp had diminished in these four areas to ∼0 with total ΔPp reaching plateaus ranging from 0.36 to 0.75 MPa. The ΔPp at the time of ES onset for these areas ranges from 0.28 to 0.36 MPa. Earthquake activity typically continued in a sporadic fashion following the initial onset in these areas, with the number of post-onset reactivations ranging from 1 to 7 with a mean additional ΔPp of 0.12 MPa between each.

The G, F, I, and L sequences are *distal* meaning that they are >20 km away from areas of multiple SWD wells with significant volumes of cumulative injection prior to, or during ES activity. These sequences are in the center of the AOI or to the north, northeast, and southeast (Figure 1). The ΔPp history of the *distal* areas is simple, reflecting gradual increases in ΔPp at the regional scale over time and without significant short-term temporal variations. The overall increase in ΔPp that these areas experienced ranged from 0.07 to 0.27 MPa and all of these areas were still experiencing increasing ΔPp as of January 2019. The onset of seismicity in these areas was associated with ΔPp ranging between remarkably low values of 0–0.07 MPa, with a mean of 0.04 MPa. The number of post-onset reactivations in these ES ranged from 0 to 9, with a mean ΔPp of 0.04 MPa between each reactivation (Table S2).

The D and DA sequences are *hybrids* showing early *proximal* behavior followed by *distal*. These 2 areas were near to 1 (D) or 2 (DA) SWD wells with active SWD early in their sequence histories. The injection then slowed or stopped, and these ESs areas evolved into the *distal* class of behavior.

The overall relationship between ES onset, reactivation, and ΔPp is complex. In the *proximal* areas, onset occurred ∼3–6 years after the start of ΔPp locally and during periods of quasi steady-state ΔPp increase. In the *distal* areas, onset occurred ∼1–9 years after the start of ΔPp locally as well as during periods of quasi steady-state ΔPp increase. Based on these observations we conclude that a minimum level of ΔPp is more indicative of rupture as compared to rate of ΔPp or, by extension, stressing rate.

3.3. Evolution of Fault Surface Criticality

In addition to finding the probabilistic FSP of fault traces along the basement-sediment interface, we deterministically estimated the evolution of fault surface area over the time that they became critically stressed due to ΔPp. For the ES faults for which we have 3D control, we find that all were subcritical prior to ΔPp from SWD. This is consistent with the lack of recorded seismicity in the FWB prior to widespread SWD. By. By the end of 2018, 1.3 km^2 of the V ES fault system had reached criticality due to ΔPp increase associated with SWD (Figure 3c). The largest V earthquake (M4) occurred in May 2015. For the A ES, aggregate fault area criticality increased to 7.0 km^2 just prior to earthquake onset in late 2013 and subsequently climbed in steps to 9.5 km^2 temporally coincident with additional reactivations of this ES (Figure 3d). No portions of the 3D surfaces of seismogenic faults in the other ES areas became critically stressed following Pp increases based on this simple deterministic approach. Taken together, we conclude that even when using comprehensive inputs, a deterministic approach to modeling fault surface criticality is difficult to parameterize given the irreducible nature of the uncertainties involved.

3.4. Evolution of Fault Slip Potential

As summarized in Table S1, the FSP of the ES areas increases with ΔPp, as expected. The V ES is a *proximal* example and yielded the highest native FSP (0.39) which increased with ΔPp to 0.45 at ES onset and to 0.58 in 2019. Taking the four *proximal* ES areas together, the mean FSP at ES onset was 0.24 and the change from native to onset for the four ESs ranged 0.02 to 0.08.

The I area is an example of a *distal* ES. The native FSP of its associated fault is 0.31, which increased to 0.35 during the period of ΔPp. The FSP at ES onset was 0.31 and therefore it too did not change appreciably as the system went from pre- to post-onset. For the *distal* ES areas taken together, the mean FSP at ES onset was 0.17 and the mean change from native to onset was negligible.

4. Conclusions

1. Approximately 9% of the trace length of faults in the AOI became seismogenic following an increase in Pp from SWD ranging from 0.01 to 0.36 MPa, indicating that faults in the FWB can be made unstable with very small stress perturbations from ΔPp.
2. Many more kilometers of fault trace length did not become seismogenic as compared to the trace length that did, at all levels of total ΔPp.
3. The response of faults is strongly heterogeneous, with many non-seismogenic faults experiencing higher ΔPp compared to those that became seismogenic. These observations indicate a wide variation in the native sensitivity of faults or the limitations of the 3D hydrogeological model.
4. Once established, reactivation of the earthquake sequences occurred with additional increases of ΔPp ranging from 0 to 0.37 MPa, with no apparent relationship between the number of reactivations and the magnitude of ΔPp associated with first onset. This is merely the ΔPp associated with continued ES activity and does not consider other important factors such as local slip-induced stress change.
5. Faults *proximal* to SWD operations became seismogenic at appreciably higher mean ΔPp than those in *distal* areas (0.31 vs. 0.04 MPa). This suggests that, as areas with increased ΔPp spread laterally and preferentially to the north and east, the most unstable *distal* faults were made to slip. A fuller understanding of the impact of poroelastic stressing from ΔPp may further inform this observation.
6. Our analysis of the evolution of stress criticality with ΔPp of the 3D fault surfaces in each of the ES areas resulted in only two with straightforward correspondence to ES onset and reactivation behavior (A and V ES). Taken together, we conclude that even when using comprehensive inputs, a deterministic approach to modeling fault surface criticality is difficult to parameterize given the irreducible nature of the uncertainties involved.
7. FSP averaged 0.24 at the time of earthquake onset in areas near SWD operations with higher associated ΔPp. FSP averaged 0.17 at the time of earthquake onset in areas away from SWD operations and lower associated ΔPp. These results strengthen the hypothesis that, as ΔPp spread throughout the basin, increasingly sensitive faults became reactivated.
8. Because the FSP program is widely used in the petroleum industry to assess the hazard of fault reactivation due to SWD and other subsurface operations, our observations of the relationship between ES development and native FSP and ΔFSP in the FWB can be used qualitatively to assess thresholds between stable and unstable faults in analogous geologic systems.
9. We find that ES onset and reactivation was generally associated with periods of steady or decreasing ΔPp. The relationship between ΔPp or ΔFSP and the rate or maximum magnitude of earthquakes hosted on the same faults is not straightforward, other than the general association of earthquakes with increases in both parameters. Stressing rate from ΔPp is not indicated as an important parameter at the scale we study.
10. At the end of 2018, Pp was no longer increasing in the ES areas *proximal* to SWD operations and only the V ES area experienced earthquakes in 2019. Pp was still increasing in the *distal* ES areas and the I and L ES areas experienced earthquakes in 2019. Even if SWD ceased throughout the basin, seismicity could reasonably expect to continue, particularly in these *distal* areas, due to ongoing Pp migration away from areas of past injection.

Acknowledgments
The authors thank Manoochehr Shirzaei, Kristin Marra, Janet Slate, and an anonymous reviewer for suggestions that greatly improved the article. Financial support provided by The State of Texas through The University of Texas Bureau of Economic Geology TexNet Seismic Monitoring Program (Hennings, Nicot, Gao, DeShon, Morris, Horne, Breton) and the industrial affiliates of the Center for Integrated Seismicity Research (Hennings), the industrial affiliates of the Stanford Center for Induced and Triggered Seismicity (SCITS; Lund Snee), and U.S. Geologic Survey National Earthquake Hazard Reduction Program Award No. G16AP00140 (Brudzinski).

Data Availability Statement

Supplemental data are archived at: https://dataverse.tdl.org/dataverse/texnet-cisr-dfw.

References

Chen, R., Xue, X., Yao, C., Datta-Gupta, A., King, M. J., Hennings, P., & Dommisse, R. (2018). *Coupled fluid flow and geomechanical modeling of seismicity in the Azle area North Texas*. Society of Petroleum Engineers. https://doi.org/10.2118/191623-MS

DeShon, H. R., Hayward, C. T., Ogwari, P. O., Quinones, L., Sufri, O., Stump, B., & Magnani, M. B. (2018). Summary of the North Texas earthquake study seismic networks, 2013-2018. *Seismological Research Letters*, *90*, 387–394. https://doi.org/10.1785/0220180269

Frohlich, C. (2012). Two-year survey comparing earthquake activity and injection well locations in the Barnett Shale, Texas. *Proceedings of the National Academy of Sciences of the United States of America*, *109*, 13934–13938. https://doi.org/10.1073/pnas.1207728109

Frohlich, C., DeShon, H., Stump, B., Hayward, C., Hornbach, M., & Walter, J. I. (2016). A historical review of induced earthquakes in Texas. *Seismological Research Letters*, *87*(4), 1022–1038. https://doi.org/10.1785/0220160016

Gao, R. S., Nicot, J.-P., Hennings, P. H., La Pointe, P., Smye, K. M., Horne, E. A., & Dommisse, R. (2021). Low pressure build-up with large disposal volumes of oilfield water: A comprehensive hydrogeologic model of pore pressure change in the Ellenburger Group, Fort Worth Basin, North-Central Texas, accepted AAPG Bulletin. Retrieved from https://archives.datapages.com/data/bulletns/aop/2021-07-07/aapgbltn20159aop.html

Gono, V., Olson, J. E., & Gale, J. F. (2015). Understanding the correlation between induced seismicity and wastewater injection in the Fort Worth Basin. American Rock Mechanics Assoc., 49th U.S. Rock Mechanics/Geomechanics Symposium, 15-00419.

Haddad, M., & Eichhubl, P. (2020). Poroelastic modeling of basement fault reactivation caused by saltwater disposal near Venus, Johnson County, Texas, American Rock Mechanics Assoc., 54th U.S. Rock Mechanics/Geomechanics Symposium, ARMA-2020-2006.

Hennings, P. H., Lund Snee, J., Osmond, J. L., DeShon, H. R., Dommisse, R., Horne, E., et al. (2019). Injection-induced seismicity and fault-slip potential in the Fort Worth Basin, Texas. *Bulletin of the Seismological Society of America*, *109*, 1615–1634. https://doi.org/10.1785/0120190017

Hornbach, M. J., Deshon, H. R., Ellsworth, W. L., Stump, B. W., Hayward, C., Frohlich, C., et al. (2015). Causal factors for seismicity near Azle, Texas. *Nature Communications*, *6*, 1–11. https://doi.org/10.1038/ncomms7728

Hornbach, M. J., Jones, M., Scales, M., DeShon, H. R., Magnani, M. B., Frohlich, C., et al. (2016). Ellenburger wastewater injection and seismicity in North Texas. *Physics of the Earth and Planetary Interiors*, *261*, 54–68. https://doi.org/10.1016/j.pepi.2016.06.012

Horne, E. A., Hennings, P. H., Osmond, J. L., & Deshon, H. R. (2020). Structural characterization of potentially seismogenic faults in the Fort Worth Basin. *Interpretation*, *8*, T323–T347. https://doi.org/10.1190/INT-2019-0188.1

Justinic, A. H., Stump, B., Hayward, C., & Frohlich, C. (2013). Analysis of the Cleburne, Texas, earthquake sequence from June 2009 to June 2010. *Bulletin of the Seismological Society of America*, *103*(6), 3083–3093. https://doi.org/10.1785/0120120336

Lund Snee, J. E., & Zoback, M. D. (2016). State of stress in Texas: Implications for induced seismicity. *Geophysical Research Letters*, *43*(19), 10208–10214. https://doi.org/10.1002/2016GL070974

Lund Snee, J.-E., & Zoback, M. D. (2018). State of stress in the Permian Basin, Texas and New Mexico: Implications for induced seismicity. *The Leading Edge*, *37*, 127–134. https://doi.org/10.1190/tle37020127.1

Magnani, M. B., Blanpied, M. L., DeShon, H. R., & Hornbach, M. J. (2017). Discriminating between natural versus induced seismicity from long-term deformation history of intraplate faults. *Science Advances*, *3*(11), e1701593. https://doi.org/10.1126/sciadv.1701593

Ogwari, P. O., DeShon, H. R., & Hornbach, M. J. (2018). The Dallas-Fort Worth airport earthquake sequence: Seismicity beyond injection period. *Journal of Geophysical Research: Solid Earth*, *123*(1), 553–563. https://doi.org/10.1002/2017JB015003

Quinones, L. A., DeShon, H. R., Jeong, S.-J., Ogwari, P., Scales, M. M., & Kwong, K. B. (2019). Tracking induced earthquakes in the Fort Worth Basin: A summary of the 2008-2018 North Texas Earthquake study catalog. *Bulletin of the Seismological Society of America*, *109*, 1203–1216. https://doi.org/10.1785/0120190057

Quinones, L. A., DeShon, H. R., Magnani, M. B., & Frohlich, C. (2018). Stress orientations in the Fort Worth Basin, Texas, determined from earthquake focal mechanisms. *Bulletin of the Seismological Society of America*, *108*(3A), 1124–1132. https://doi.org/10.1785/0120170337

Scales, M. M., DeShon, H. R., Magnani, M. B., Walter, J. I., Quinones, L., Pratt, T. L., & Hornbach, M. J. (2017). A decade of induced slip on the causative fault of the 2015 Mw4.0 Venus Earthquake, Northeast Johnson County, Texas. *Journal of Geophysical Research: Solid Earth*, *122*(10), 7879–7894. https://doi.org/10.1002/2017JB014460

Skoumal, R. J., Brudzinski, M. R., & Currie, B. S. (2015). Distinguishing induced seismicity from natural seismicity in Ohio: Demonstrating the utility of waveform template matching. *Journal of Geophysical Research*, *120*, 6284–6296. https://doi.org/10.1002/2015JB012265

Skoumal, R. J., Brudzinski, M. R., Currie, B. S., & Levy, J. (2014). Optimizing multi-station earthquake template matching through re-examination of the Youngstown, Ohio Sequence. *Earth and Planetary Science Letters*, *405*, 274–280. https://doi.org/10.1016/j.epsl.2014.08.033

Smye, K. M., Lemons, C. R., Eastwood, R., McDaid, G., & Hennings, P. H. (2019). Stratigraphic architecture and petrophysical characterization of formations for deep disposal in the Fort Worth Basin, TX, *Interpretation*, 1–52. https://doi.org/10.1190/INT-2018-0195.1

Walsh, F. R., & Zoback, M. D. (2016). Probabilistic assessment of potential fault slip related to injection induced earthquakes: Application to north-central Oklahoma, USA. *Geology*, *44*(12), 991–994. https://doi.org/10.1130/G38275.1

Walsh, F. R. I., Zoback, M. D., Pais, D., Weingartern, M., & Tyrrell, T. (2017). *FSP 1.0: A program for probabilistic estimation of fault slip potential resulting from fluid injection*. Retrieved from https://scits.stanford.edu/software

Zhai, G., & Shirzaei, M. (2018). Fluid injection and time-dependent seismic hazard in the Barnett Shale, Texas. *Geophysical Research Letters*, *45*, 4743–4753. https://doi.org/10.1029/2018GL077696

Reference From the Supporting Information

Schaff, D. P., & Richards, P. G. (2014). Improvements in magnitude precision, using the statistics of relative amplitudes measured by cross correlation, *Geophysical Journal International*, *197*(1), 335–350. https://doi.org/10.1093/gji/ggt433